Catalysis Today 179 (2012) 61–72

Contents lists available at ScienceDirect

Catalysis Today

journal homepage: www.elsevier.com/locate/cattod

Aromatization of alkanes over Pt promoted conventional and mesoporous gallosilicates of MEL zeolite

M.N. Akhtar[a], N. Al-Yassir[a], S. Al-Khattaf[a,*], Jiří Čejka[b,**,1]

[a] KAUST Center in Development, King Fahd University of Petroleum and Minerals, Dhahran 31261, Saudi Arabia
[b] J. Heyrovský Institute of Physical Chemistry, Academy of Sciences of the Czech Republic, v.v.i., Dolejškova 3, 182 23 Prague 8, Czech Republic

ARTICLE INFO

Article history:
Received 28 April 2011
Received in revised form 31 May 2011
Accepted 1 June 2011
Available online 28 July 2011

Keywords:
Alkane aromatization
ZSM-11
GaHZSM-11
Desilication
Intracrystalline mesoporosity
Platinum

ABSTRACT

Aromatization of hexane and propane was investigated over Pt promoted mesoporous gallium-containing HZSM-11 with controlled mesoporosity generated by desilication. Prepared catalysts were characterized by nitrogen adsorption, X-ray powder diffraction, scanning electron microscopy, Fourier transform infrared of chemisorbed pyridine, and NH_3 temperature programmed desorption confirming the development of intracrystalline mesoporosity of Ga-containing HZSM-11. The catalytic activities, which were compared in the aromatization of *n*-hexane and propane, increased upon desilication. The aromatization of *n*-hexane decreased in the following order, Pt/mesoporous GaZSM-11 ≫ Pt/conventional GaZSM-11 ≫ mesoporous GaZSM-11 > conventional GaZSM-11. Hexane conversion reached 70.1% over mesoporous Pt/GaZSM-11 with Si/Ga of 61, as compared with 29.6 and 24.9% for corresponding mesoporous and conventional GaZSM-11 (Si/Ga = 94), respectively, for experiments at liquid hour space velocity of 3.6 h^{-1}, and 540 °C. Comparison of BTX (benzene–toluene–xylene) selectivity at the conversion level of ~21.0% revealed that Pt/mesoporous GaZSM-11 is more selective than corresponding mesoporous and conventional GaZSM-11. The BTX selectivity over Pt/mesoporous GaZSM-11 (Si/Ga = 94), which showed strong dependence on the conversion, reached 28.2%, whereas over corresponding mesoporous and conventional GaZSM-11catalysts reached 19.1% and 5.5%, respectively. A higher conversion and better selectivity can be attributed to the improved accessibility to the active extra-framework Ga species owing to the generation of mesopores inside the zeolite particles and shortening the contact time. It is worth mentioning that the prepared catalysts exhibited quite low activity in propane aromatization but exhibiting similar trends as for hexane aromatization.

1. Introduction

Transformation of alkanes into higher value products, in particular aromatization of linear alkanes into BTX aromatics (benzene, toluene, and xylene) has been the subject of interest for last decades [1]. This stems from the wide applications of BTX. They are used as blending mixture to enhance the octane number of gasoline, and are essential raw chemicals for the petrochemical industry (i.e. aromatics represent about 30% of the some 8 million known organic compounds [2]). Benzene is widely used in downstream chemical processes such as production of styrene and phenol, whereas xylenes are essential for production of purified terephthalic acid and isophthalic acid [3]. Indeed, the presence of commercial processes for alkane aromatization (i.e. M-2 Forming (Mobil), Cyclar (BP-UOP), Z-forming (Mitsubishi), and Alpha process (SandyAsahi)) bears testimony to the economic importance of the aromatization process [4–6].

Particular research effort has been directed to gallium-containing medium pore zeolites owing to the unique properties of ZSM-5 including uniform dimensions of pore channel, intrinsic acidity, and ability to confine active metals [7–22]. Zeolites MCM-22 [23], Beta [24], mesoporous silicate [25] and structured zeolites [26] were also investigated, while metals such as Pt [4,6,18,27,28], Zn [4,6,19,29,30] and to a lower extent Cu [31], Re [32], Co [33] and Ge [34] have received some attention. The main drawback of Ga-containing HZSM-5 is a low dispersion degree of extra framework Ga species, which have been demonstrated in many studies, to adversely affect the BTX selectivity. It is generally accepted that it is quite difficult to incorporate Ga^{3+} ions into HZSM-5 via methods such as impregnation or physical admixture, as compared with other metal cations. This is largely due to highly positive electrostatic charge and the size of gallium aquacomplexes coupled with the hydrophobicity and weak anion field of ZSM-5

* Corresponding author. Fax: +966 3 860 4234.
** Corresponding author. Fax: +420 28658 2307.
E-mail addresses: skhattaf@kfupm.edu.sa, skhattaf@hotmail.com (S. Al-Khattaf), jiri.cejka@jh-inst.cas.cz (J. Čejka).
[1] Joint Professor of the Center of Research Excellence in Petroleum Refining and Petrochemicals, King Fahd University of Petroleum and Minerals, Dhahran 31261, Saudi Arabia.

0920-5861/$ – see front matter © 2011 Elsevier B.V. All rights reserved.
doi:10.1016/j.cattod.2011.06.036

framework [35,36]. This would hinder their effective penetration into zeolite micropores and subsequent interaction with Brönsted sites. Hence, Ga^{3+} cations would reside predominantly on the external zeolite surface as extracrystalline Ga_2O_3. However, it has been shown by several studies that Ga ions can be properly dispersed as extra-framework species in zeolite micropores (true ion-exchange) [9,15–17]. These methods, including ion-exchange, reducing-oxidizing pretreatment cycles and chemical vapor deposition, resulted in an effective deposition of cationic gallium species directly into the micropores replacing Brønsted sites. Recently, we have shown that incorporation of Ga into ZSM-5 via hydrothermal synthesis significantly improved the aromatization performance [37]. This was attributed to the uniform distribution of Ga species throughout the zeolite channels.

An alternative approach to further improve the aromatization performance of Ga-containing zeolite is to introduce intracrystalline mesoporosity in zeolite crystals, which would shorten the contact time of reaction intermediates. The microporous character of zeolite often leads to intracrystalline diffusion limitations on the reaction rate, and thus adversely affects catalytic performance [38]. It has been shown that diffusion limitations decrease upon decreasing the size of zeolite crystals [39]. Alternatively, intracrystalline mesoporosity in zeolite crystals can be introduced by post-synthesis modifications such as dealumination (i.e. acid leaching, steaming) [40] and desilication (alkaline treatment) [41,42], or by direct carbon templating method [26,43]. Other methods include composite microporous/mesoporous materials [44], zeolite delamination [45], and synthesis of wide-pore zeolite [46]. There are scarce reports about the role of zeolite mesoporosity on the aromatization reactions. Song et al. [47] showed that the catalytic stability of ZSM-5 in butene aromatization was improved by the treatment of ZSM-5 with NaOH solution. They attributed that to the generation of new mesopores resulting from a preferential removal of Si^{4+} species. Leth et al. [26] examined the effect of zeolite mesoporosity in ethane conversion. They showed that conventional and mesoporous GaZSM-5 (Si/Ga = 43, and 38, respectively) differed greatly in ethane conversion, as a result of different mesoporosity, with higher conversion for mesoporous GaZSM-5.

The aim of this work was the investigation of the role of intracrystalline mesoporosity of GaZSM-11 on the aromatization of linear alkane. Ga-containing ZSM-11 was prepared by hydrothermal synthesis. Mesopores were obtained by alkaline treatment (desilication) of GaZSM-11. Galloaluminosilicate (Ga,AlZSM-5) was examined for comparison. Textural, structural, and morphological properties of catalysts under study were evaluated by N_2 sorption, FTIR, XRD and SEM. The acidic properties were examined by FTIR of chemisorbed pyridine and NH_3–TPD. The catalytic properties of all synthesized samples were evaluated during the aromatization of propane and *n*-hexane.

2. Experimental

2.1. Materials

Sodium silicate solution (SiO_2: 27 wt%), tetraethyl orthosilicate, $Al_2(SO_4)_3{\cdot}14–18H_2O$, $Al(NO_3)_3{\cdot}9H_2O$ $Ga(NO_3)_3{\cdot}8H_2O$, tetrapropylammonium bromide, tetrabutylammonium hydroxide, H_2SO_4, NaOH, NaCl, and NH_4NO_3 and β-Ga_2O_3 were obtained from Aldrich and were used as supplied without any further purifications.

2.2. Zeolite synthesis and modification

2.2.1. Hydrothermal synthesis of parent zeolite

2.2.1.1. ZSM-11. ZSM-11 (Si/Al = 35) was prepared using tetrabutyl ammonium bromide as structure directing agent. In the typical synthesis, 51 g of tetraethyl orthosilicate was slowly added to the solution containing 2.62 g of aluminum nitrate nonahydrate and 26 g of water. Afterwards, 0.51 g of sodium hydroxide dissolved in 21.4 g of water was added dropwise to the above solution. 31.45 g of tetrabutyl ammonium hydroxide and 34 g of water is added to the reaction mixture under vigorous stirring. The crystallization is carried out under agitation in Teflon-lined autoclaves at 170 °C for 6 days. The resulting solid phase is recovered by filtration, extensively washed out with distilled water (0.5 L) and dried at 90 °C overnight. Calcination is carried out in air at 550 °C for 8 h (1 °C/min). Ammonium forms of these zeolites were prepared via four-time repeated ion-exchange (4.5 h) of sample in 1.0 M aqueous solution of ammonium nitrate.

2.2.1.2. AlZSM-5. AlZSM-5 (Si/Al = 86) was synthesized by hydrothermal crystallization from a gel consisting of sodium silicate, aluminum sulphate, tetrapropyl ammonium bromide, gallium nitrate, sulfuric acid, and deionized water in a stainless steel autoclave at 180 °C for 72 h. The thermal treatment (calcination, drying, calcination, and deammonation) was similar to that of ZSM-11.

2.2.2. Hydrothermal synthesis of Ga-containing zeolite

2.2.2.1. GaZSM-11 (Gallosilicate). GaZSM-11 was synthesized by hydrothermal crystallization from a gel consisting of tetraethyl orthosilicate, gallium nitrate, sodium hydroxide, tetrabutyl ammonium hydroxide and deionized water in a Teflon-lined autoclave at 170 °C for 7 days. After crystallization, the solid phase was filtered off, washed out and dried at 90 °C overnight. The template was removed by calcination at 550 °C for 8 h with the temperature ramp of 1 °C/min. The acid form of GaZSM-11 was obtained by four times repeated ion-exchange with 1.0 M ammonium nitrate. Then, the solid was then filtered, washed, dried at 120 °C for 3 h and calcined at 550 °C for 3 h. GaZSM-11(94) is noted as conventional GaZSM-11, where the number in parenthesis corresponds to Si/Ga molar ratio.

2.2.2.2. Ga,AlZSM-5 (Galloaluminosilicate). The galloaluminosilicate (Ga,AlZSM-5) was synthesized by hydrothermal crystallization from a gel (pH 10) consisting of sodium silicate, aluminum sulphate, tetrapropylammonium bromide, gallium nitrate, sulfuric acid, and deionized water in a stainless steel autoclave at 180 °C for 72 h. In a typical synthesis, two separate solutions were prepared for the synthesis of galloaluminosilicate Ga,AlZSM-5. The first solution was obtained by diluting a known amount of sodium silicate solution in deionized water. The second solution was obtained by adding a known amount of gallium nitrate, tetrapropyl ammonium bromide, H_2SO_4 (98%), and NaCl in deionized water. The two solutions were mixed and stirred vigorously at ambient temperature for 1 h. The resulting gel mixture was transferred into 100 ml Teflon cup inserted in stainless steel autoclave, which was then rotated in an oven (13–14 rpm) heated at 180 °C for 72 h. After the completion of the synthesis, the crystalline product was washed repetitively with deionized water, dried at 120 °C for 3 h, and then calcined at 550 °C for 3 h (heating rate 5 °C/min). The acid form of GaZSM-11 was obtained by four times repeated ion-exchange with 1.0 M ammonium nitrate. Then, the solid was then filtered, washed, dried at 120 °C for 3 h and calcined at 550 °C for 3 h. Then, the solid was then filtered, washed, dried at 120 °C for 3 h and calcined at 550 °C for 3 h. Ga,AlZSM-5(84) is noted as galloaluminosilicate, where the number in parenthesis corresponds to Si/(Al + Ga) ratio.

2.2.3. Desilication of GaZSM-11

The GaZSM-11 (Si/Ga = 94) was treated with the 0.2 M solution of NaOH for two hours. The sample was then filtered off, thoroughly

washed with distilled water, dried at 60 °C overnight. GaZSM-11(61) obtained by desilication is noted as mesoporous GaZSM-11, where the number in parenthesis corresponds to Si/Ga ratio.

2.2.4. Impregnation of Pt onto zeolites

All zeolites were modified with 0.5 wt. % Pt using wet impregnation method. In a typical procedure a certain amount of 0.5 wt % aqueous solution of $Pt(NH_3)_4(NO_3)_2$ was added to the required amount of zeolite. The zeolite was left overnight to equilibrate. Then water was removed in a vacuum oven and catalyst was dried and calcined at 120 °C and 550 °C, respectively, for 3 h.

2.3. Characterization of catalysts

The chemical compositions (Si, Al, and Ga) of synthesized samples were determined by atomic absorption spectroscopy, using the Perkin-Elmer equipment (Model A. Analyst 100).

The textural properties were characterized by N_2 adsorption measurements at 77 K, using Quantachrome Autosorb 1-C adsorption analyzer. Samples were outgassed at 220 °C under vacuum (10^{-5} Torr) for 2 h before N_2 physisorption. The S_{BET} surface areas were determined from the adsorption data in the relative pressure (P/P_0) range from 0.06 to 0.2, assuming a value of 0.164 nm^2 for the cross-section of the N_2 molecule.

X-ray diffraction (XRD) patterns were recorded on a Rigaku Miniflix II XRD powder diffraction system using CuK(radiation (($_{K(1}$ = 1.54051 Å, 30 kV and 15 mA). The XRD patterns were recorded in the static scanning mode from 5–60° (2() at a detector angular speed of 2°/min and step size of 0.02°.

Scanning Electron Microscopy (SEM) images were performed on selected samples to determine the crystallite size and morphology. The SEM images were recorded using Philips XL30 SEM.

Infrared spectroscopy of adsorbed pyridine was used to determine the types of acid sites present. The measurements were carried out using a Fourier transform infrared Bruker Equinox 55 spectrometer with a resolution of 2 cm^{-1} and an MCT detector. All samples were activated in a form of self-supporting wafers (ca. 5 mg/cm^2) at 450 °C under vacuum for 1 h prior to the adsorption of pyridine. The adsorption temperature of pyridine was 170 °C. All measured spectra were recalculated to a "normalized" wafer of 10 mg. For a quantitative characterization of acid sites, the following bands and absorption coefficients were used: pyridine (PyH^+) band at 1545 cm^{-1}, ε = 0.078 cm/μmol^{-1}; pyridine (PyL) bands at 1461 and 1454 cm^{-1}, ε = 0.165 cm/μmol^{-1} [48a,b].

Temperature-programmed desorption of NH_3 (NH_3–TPD) was carried out using Quantachrome Autosorb 1-C/TCD. Samples were pretreated at 450 °C in a flow of helium (50 ml min^{-1}) for 2 h. This was followed by the adsorption of ammonia (5 vol.% in helium) at 100 °C for 30 min. Samples were then purged in a He stream for 2 h at 120 °C in order to remove loosely bound ammonia (i.e. physisorbed and H-bonded ammonia). Then, the samples were heated again from 100 to 700 °C with a heating rate of 10 °C/min in a flow of helium (25 ml min^{-1}) while monitoring the evolved ammonia using TCD.

2.4. Catalytic experiments

The aromatization of propane and *n*-hexane over different catalysts was carried out in a fixed bed tubular reactor. In a typical experiment, the reactor was charged with 1.0 ml of catalyst previously pelletized, and sieved to a particle size of 0.5–1.00 mm diameter. The feed propane or *n*-hexane was mixed with N_2. The ratio of N_2 to C_3 feed was 2:1 with the GHSV (gas hour space velocity) of 1600 h^{-1}. In case of *n*-hexane feed, the LHSV was maintained at 3.6 h^{-1} while GHSV of N_2 was maintained at 300 h^{-1}. The reaction temperature was maintained at 540 °C during 5 h time-on-stream (TOS) under atmospheric pressure. The LHSV of *n*-hexane was varied within the range of 3.6–32.4 h^{-1}.

The platinum incorporated catalysts were first reduced under flow of hydrogen at 450 °C for 3 h before introduction of feed. The quantitative analysis of the reaction products was carried out on line using Varian GC with FID (Varian 450-GC), equipped with an HP-INNOWax capillary column (Polyethylene glycol (PEG)) (length 60 m × internal diameter 0.32 mm × film thickness 0.50 μm).

3. Results and discussion

3.1. Chemical composition, structural, textural and morphological properties

Table 1 shows chemical composition of all Ga-containing zeolites (ZSM-11 and ZSM-5) used in this study. It can be noted that the Si/Ga ratio of GaZSM-11 decreased upon desilication performed in an alkaline solution (Si/Ga decreased from 94 (conventional GaZSM-11) to 61 for mesoporous GaZSM-11).

XRD patterns of the conventional and mesoporous GaZSM-11 and Pt promoted samples are shown in Fig. 1. All samples showed characteristic XRD reflections of HZSM-11 (MEL type) [49] and confirm that all samples, including the mesoporous GaZSM-11 (desilicated), were highly crystalline as suggested by the sharpness of XRD reflection in the 22.5–25.0° 2θ range. The calculated degree of crystallinity was over 95% for all zeolites studied (Table 2). In

Table 1
Chemical composition of Pt promoted gallium-containing zeolite.

Catalysts	Chemical analysis by AAS[a]		
	Pt (wt%)	Si/Al	Si/Ga
Conventional GaZSM-11(94)	0.5	–	94
Conventional GaZSM-11(91)	0.5	–	91
Mesoporous GaZSM-11(61)	0.5	–	61
Pt/Conventional GaZSM-11(94)	0.5	–	94
Pt/Conventional GaZSM-11(92)	0.5	–	92
Pt/mesoporous GaZSM-11(67)	0.5	–	67
ZSM-5 (86)	0.5	94	–
GaZSM-5(84)*	0.5	136	373
PtGaZSM-5(84)*	0.5	136	361

[a] By Atomic Absorbance Spectroscopy (AAS).
* Number in parenthesis corresponds to Si/(Al + Ga).

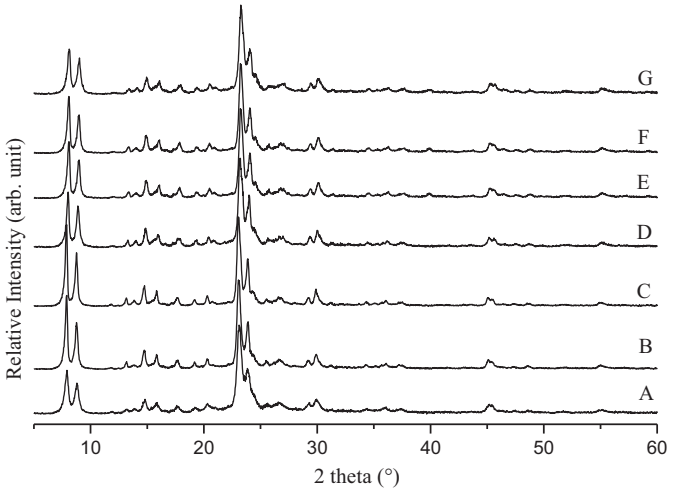

Fig. 1. XRD patterns of Pt promoted Ga-containing HZSM-11; (A) HZSM-11, (B) conventional GaZSM-11(Si/Ga = 94), (C) conventional GaZSM-11(Si/Ga = 91), (D) mesoporous GaZSM-11(Si/Ga = 61), (E) Pt/conventional GaZSM-11(Si/Ga = 94), (F) Pt/conventional GaZSM-11(Si/Ga = 92), and (G) Pt/mesoporous GaZSM-11 (Si/Ga = 67).

Table 2
Textural and structural properties of Pt promoted gallium-containing zeolite.

Catalysts	Relative Crsyst.[a]	Textural properties					
	XRD	S_{BET} ($m^2\ g^{-1}$)	S_{meso} ($m^2\ g^{-1}$)[b,c]	V_{total} (cm^3/g)	V_{micro} (cm^3/g)[b]	V_{meso} (cm^3/g)[b]	V_{meso}/V_{mico}
Conventional GaZSM-11(94)	100	451	32.0	0.27	0.22	0.05	0.23
Conventional GaZSM-11(91)	100	352	25.0	0.22	0.17	0.05	0.29
Mesoporous GaZSM-11(61)	99	489	218	0.53	0.14	0.39	2.78
Pt/Conventional GaZSM-11(94)	100	365	29.0	0.23	0.17	0.06	0.36
Pt/Conventional GaZSM-11(92)	100	343	22.0	0.20	0.17	0.03	0.18
Pt/Mesoporous GaZSM-11(67)	100	370	163	0.40	0.11	0.29	2.63
AlZSM-5(86)	94	361	53.0	0.25	0.15	0.10	0.67
Ga,AlZSM-5(84)	91	416	11.0	0.27	0.20	0.07	0.35
Pt/Ga,AlZSM-5(84)	91	300	87.0	0.26	0.11	0.15	1.37

[a] Relative crystallinity based on XRD results.
[b] From *t*-plot method.
[c] S_{meso} includes the mesoporous and macroporous surface area as well as contribution from external surface. V_{meso} – for all conventional zeolites, this means interparticle volume while for Mesoporous GAZSM-11, this is volume of mesopores.

addition, no diffraction lines belonging to segregated bulk β-Ga_2O_3 were resolved in the XRD patterns [50]. Careful examination of the characteristic diffraction lines of Ga-containing HZSM-11 structure in the 2θ range of 23–25° did not reveal any change in the peak position, which often indicates expansion of zeolite unit cell upon desilication. Ohayon et al. [51] and Zhu et al. [52] reported that there was a slight shift in the position of diffraction lines of ZSM-5 zeolite to lower angle upon desilication in alkaline medium (NaOH, Na_2CO_3). Fig. 2, showing the XRD patterns of ZSM-5 and corresponding galloaluminosilicate (Ga,AlZSM-5) and Pt promoted samples, also confirms the presence of highly crystalline materials with MFI structure [49].

The textural properties of GaZSM-11 are summarized in Table 2. The N_2 adsorption–desorption isotherms of parent zeolites (not reported here for all samples) exhibited type I isotherm with a plateau at higher temperature as a result of the microporous nature of the material with a limited mesoporosity. Upon desilication (alkaline treatment) of GaZSM-11, the material showed an enhanced uptake of N_2 at higher relative pressure ($P/P_0 > 0.5$), accompanied by a hysteresis loop, being indicative of intracrystalline mesoporosity (Fig. 3) [53]. The BJH pore size distribution (BJH PSD) derived from the adsorption branch of the isotherms confirmed the presence of intracrystalline mesopores with a medium diameter of 13 nm (inset of Fig. 3). From the increase in the V_{meso}/V_{micro} ratio upon desilication (0.23 for conventional GaZSM-11) to 2.78 (mesoporous GaZSM-11) an improvement of the mass transport properties of the mesoporous GaZSM-11 can be expected.

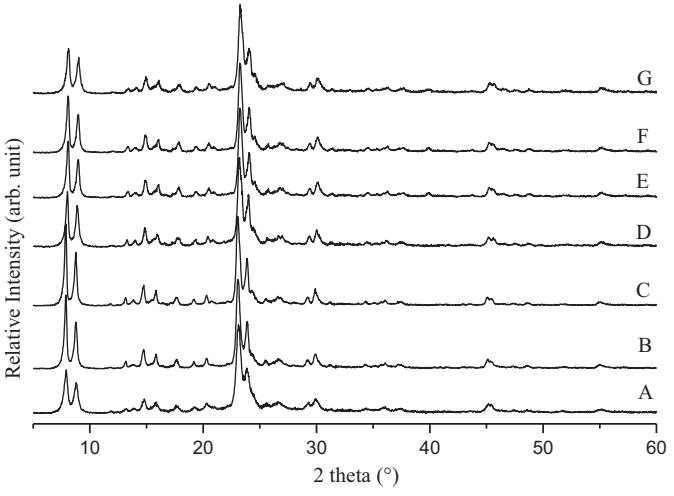

Fig. 2. XRD patterns of Pt promoted Ga,AlZSM-5; (A) AlZSM-5 (84), (B) galloaluminosilicate Ga,AlZSM-5(86), and (C) Pt/galloaluminosilicate Ga,AlZSM-5(86).

The scanning electron micrographs (SEM) of parent HZSM-11, and conventional and mesoporous GaZSM-11 are shown in Fig. 4. As evidenced by SEM, all materials are well crystalline and exhibit hexagonal prismatic crystals morphology (about 0.5 μm). Upon gallination or desilication, there was no drastic change of the morphology.

3.2. Acidic properties

The total number of acid sites and acid strength distribution of conventional and mesoporous GaZSM-11, and Pt promoted samples were determined by the temperature programmed desorption of NH_3 (Fig. 5, and Table 3). The acidity is associated with different types of acid sites that include bridged silanol groups (i.e. Si–OH–Al), and gallium species (i.e. framework (Si–OH–Ga) and extra framework species), as well as Lewis sites (coordinatively unsaturated sites). The study on the variation of surface acidity by NH_3–TPD showed a slight change in the number and properties of acid sites after alkaline treatment (desilication). The total acidity of conventional GaZSM-11 was 0.48 mmol $NH_3\ g^{-1}$, while

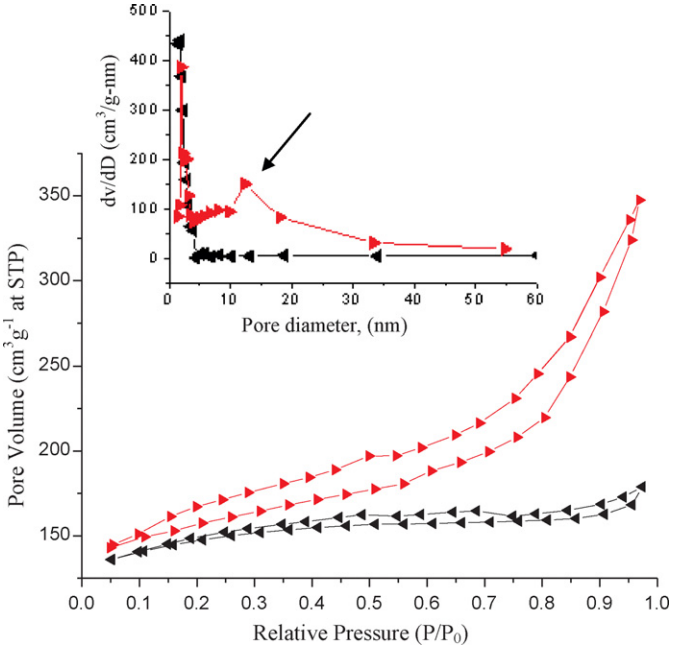

Fig. 3. N_2 adsorption–desorption isotherms of Conventional (♦) conventional GaHZSM-11(94) and (▲) mesoporous Ga-containing HZSM-11(61) (inset: pore size distribution).

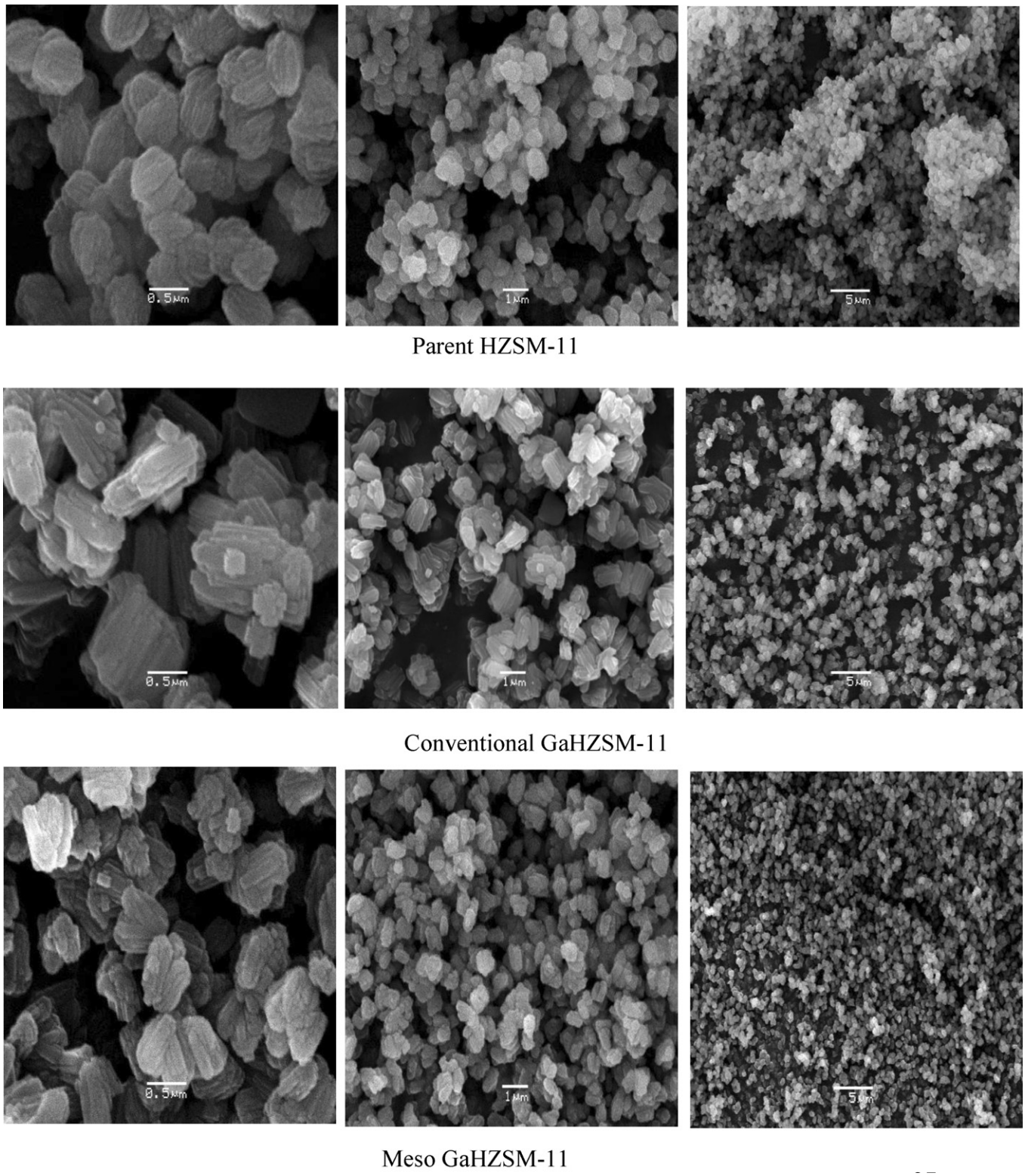

Fig. 4. SEM micrographs of parent ZSM-11 zeolite, conventional GaZSM-11(94) and mesoporous GaZSM-11(61).

upon desilication, the number increased to 0.57 mmol NH_3 g^{-1} (Table 3). All NH_3–TPD profiles were characterized by two desorption peaks with maxima in the temperature regions 201–214 and 371–386 °C, which can be assigned to NH_3 desorption from weak (physisorption) and strong acid sites, respectively (Fig. 5). Compared with conventional GaZSM-11 (untreated), the number of weak and strong acid sites on the desilicated sample increased. The ratio of strong/weak acid sites increased from 0.71 (conventional GaZSM-11) to 0.83 upon desilication.

FTIR spectra of chemisorbed pyridine for conventional and mesoporous GaZSM-11 are depicted in Fig. 6, and the concentrations of acid sites are summarized in Table 3. The bands used in this study to quantify separately the Brønsted and Lewis acid sites are the peaks around 1546 and 1446–1457 cm^{-1}, corresponding

Table 3
Summary of acid sites properties of Pt promoted gallium-containing zeolite.[a]

Zeolite	Acid density by NH_3-TPD (mmol NH_3 g^{-1})		
	Total	L.T.P.	H.T.P.
Conventional GaZSM-11(94)	0.48	0.28 (214)	0.20 (376)
Conventional GaZSM-11(91)	0.51 (0.179)[b]	0.28 (203)	0.23 (371)
Mesoporous GaZSM-11(61)	0.57 (0.198)[b]	0.30 (207)	0.25 (381)
Pt/Conventional GaZSM-11(94)	0.57	0.30 (206)	0.27 (379)
Pt/Conventional GaZSM-11(92)	0.55	0.29 (198)	0.26 (374)
Pt/mesoporous GaZSM-11(67)	0.64	0.33 (213)	0.31 (386)

[a] L.T.P and H.T.P correspond to low- and high-temperature desorption peak, respectively, and number in parenthesis corresponds to peak maximum.
[b] Number corresponds to total acid sites determined by FTIR of chemisorbed pyridine.

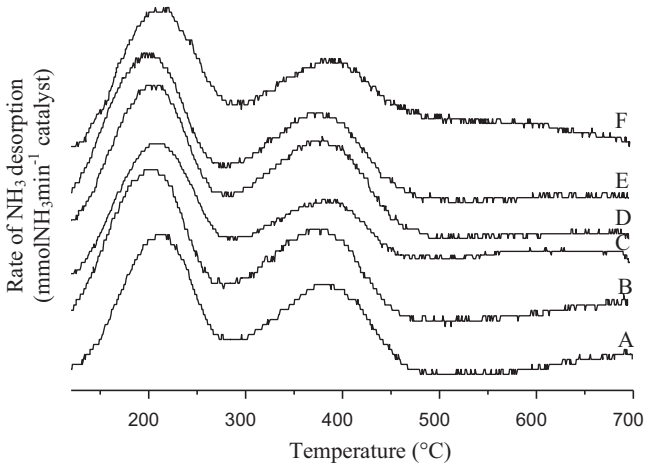

Fig. 5. NH_3–temperature-programmed desorption (NH_3–TPD) profiles of Pt promoted Ga-containing HZSM-11; (A) conventional GaZSM-11(Si/Ga = 94), (B) conventional GaHZSM-11(Si/Ga = 91), (C) mesoporous GaHZSM-11(Si/Ga = 61), (D) Pt/conventional GaZSM-11(Si/Ga = 94), (E) Pt/conventional GaZSM-11(Si/Ga = 92), and (F) Pt/mesoporous GaHZSM-11 (Si/Ga = 61).

to Z–O–HPy^+ (framework Ga species (i.e. bridged Si–OH–Ga), and Z–$Ga^{-\delta}$ $Py^{+\delta}$ (extra framework Ga species)), respectively. Although, the pattern of change in the number of acid sites corresponds well to that obtained by TPD of NH_3 (increasing in the total number of acid sites), the measured total number of acid sites was lower. The bulky size of pyridine molecule can contribute to the lower number of acid sites. Fig. 6 showed that all samples exhibited both Brønsted and Lewis sites. The concentration of Lewis acid sites for conventional GaZSM-11 upon desilication increased slightly (56%, as compared to 53% for conventional GaZSM-11). Whereas, that of Brønsted acid sites decreased (44%, as compared to 47% for conventional GaZSM-11). Fig. 6(A) showed that the peak at ca. 3745 cm^{-1} (terminal silanol groups (Si–OH) at the external of the zeolite) increased upon desilication. This implies that there is an increase in the external surface area (i.e. mesoporosity), which further supports the N_2 sorption data (Table 2).

3.3. Aromatization activity

3.3.1. Effect of desilication

The results of *n*-hexane aromatization over conventional GaZSM-11, mesoporous GaZSM-11, Pt/GaZSM-11 and Pt/mesoporous GaZSM-11 are presented in Table 4. The conventional GaZSM-11 resulted in 25% conversion of *n*-hexane with aromatic yield of 4% only. However on desilication of conventional GaZSM-11 the conversion of *n*-hexane was increased to 30% and

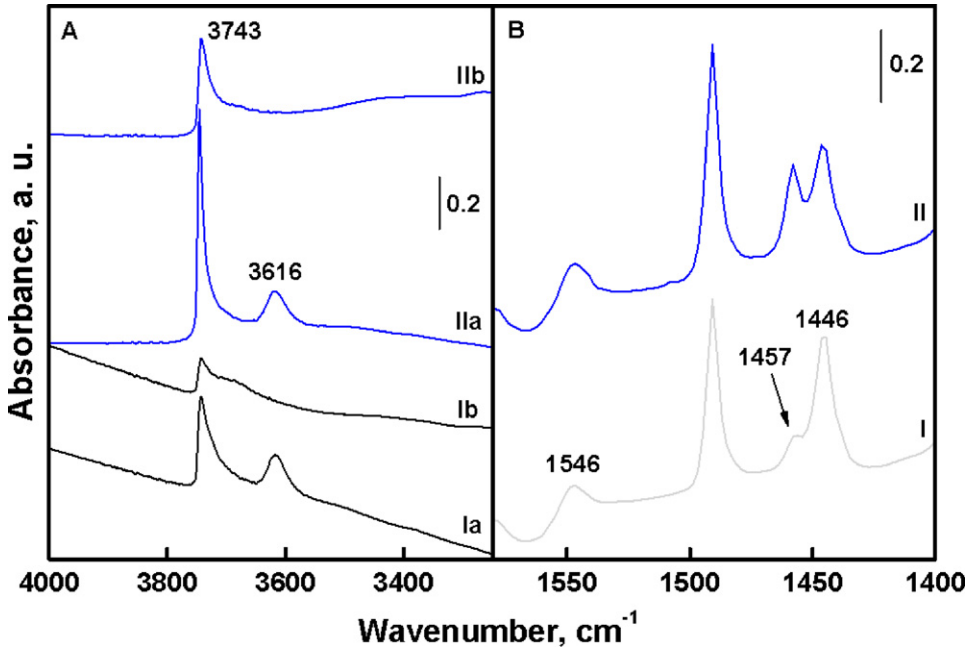

Fig. 6. FTIR spectra of conventional GaZSM-11 (I) and mesoporous GaZSM-11 (II); (a) before pyridine adsorption, (b) after adsorption of pyridine. (A) Region of hydroxyl groups, (B) region of Lewis (L) and Brønsted (B) acid sites.

Table 4
Influence of desilication of GaZSM-11 on n-hexane aromatization at 540 °C, atmospheric pressure, LHSV of 3.6 h^{-1}, and TOS of 5 h.

Catalysts	Conventional GaHZSM-11(94)	Mesoporous GaHZSM-11(61)	Pt/conventional GaHZSM-11(94)	Pt/mesoporous GaHZSM-11(67)
Conversion (%)	24.9	29.6	46.3	70.1
Aromatic (Ar) yield (%)	3.64	8.45	12.1	26.5
Product selectivity (%)				
C_1	1.67	0.57	2.19	1.38
$C_2^=$	8.32	1.35	7.12	1.52
C_2	7.37	9.64	3.64	14.2
$C_3^=$	34.5	30.0	13.3	12.9
C_3	11.5	20.5	10.9	17.4
C_4	4.01	1.98	4.24	2.52
i-C_4	2.00	0.61	11.1	3.69
$C_4^=$	15.7	9.05	11.3	6.78
C_5^+	0.56	0.23	7.92	2.05
Aromatics	14.4	26.1	28.4	37.6
Ar. distribution (%)				
Benzene	28.3	16.3	18.5	40.3
Toluene	34.5	44.7	22.1	27.9
Xylene	2.53	2.26	4.82	2.78
Ethylbenzene	22.5	22.2	21.7	14.7
C_9^+ aromatics	12.2	14.6	32.9	14.3

aromatic yield was increased to 8%. The conversion of *n*-hexane and yield of aromatics was further increased when both zeolites were impregnated with platinum. The conversion of *n*-hexane was increased from 25% to 46% on incorporation of platinum on conventional GaZSM-11. The aromatic yield was also increased from 4% to 12%. Similarly the conversion of *n*-hexane was increased from 30% to 70% on incorporation of platinum on mesoporous GaZSM-11. The aromatic yield was also increased from 8% to 27%. The conversion of *n*-hexane was in order Pt/mesoporous GaZSM-11 > Pt/conventional GaZSM-11 > mesoporous GaZSM-11 > conventional GaZSM-11. The aromatic yield was observed to be maximum for Pt/mesoporous GaZSM-11 while minimum for conventional GaZSM-11.

It is well known [54] that the product distribution during alkane aromatization is dependent on the conversion of *n*-hexane. Therefore, product distribution should be compared at the same conversion level. The results of *n*-hexane aromatization at the same conversion level (~21%) for all catalysts are presented in Table 5 and Fig. 7. It was observed that selectivity to C_1–C_3 paraffins over conventional GaZSM-11 decreased from ~26% to ~ 8% after desilication. In contrast, the selectivity to aromatic products increased from ~6% to 19%. It should be noted that toluene was preferentially (41%) produced over benzene (30%) when using conventional GaZSM-11 while the opposite trend was found for mesoporous GaZSM-11. The amount of benzene formed was 62% being much higher than for toluene (15%). It could be inferred that formation of benzene is favored for shorter contact times. We have also plotted the ratios of benzene/toluene and i-C_4/n-C_4 in Fig. 7. It has been observed that the ratio of benzene/toluene is <1 over conventional GaZSM-11 while it has increased to >4 over mesoporous GaZSM-11. Similarly the ratio of i-C_4/n-C_4 over conventional GaZSM-11 was <0.5 while on mesoporous GaZSM-11 it has increased to >3.

The presence of intracrystalline mesopores in zeolite structure enhances the transport of molecules and results in higher conversions It has been reported [55,56] that gallosilicates possess two types of gallium species (the framework and extra-framework). The extra-framework gallium species are produced during calcination of zeolite. It was widely reported [57] that the aromatization of alkanes over gallium containing zeolites and gallosilicates proceed via a bifunctional mechanism, i.e. (1) the Brønsted sites provided by the framework gallium and (2) the Lewis sites provided by extra-framework Ga_2O_3 species. Based on that it is expected that desilication might have increased the concentration of extra-framework Ga_2O_3 species. Therefore, mesopores as well as extra framework gallium species are responsible for increase in catalytic conversion and aromatic selectivity.

Table 5
n-Hexane aromatization over Pt promoted Ga-containing HZSM-11 at the same conversion level (540 °C, atmospheric pressure, and TOS of 5 h).

Catalysts	Conventional GaHZSM-11(94)	Mesoporous GaHZSM-11(61)	Pt/conventional GaHZSM-11(94)	Pt/mesoporous GaHZSM-11(67)
Conversion (%)	19.5	23.1	19.4	21.4
Aromatic (Ar) yield (%)	1.10	4.40	1.70	6.00
Product selectivity (%)				
C_1	1.95	1.38	0.55	1.95
$C_2^=$	8.05	13.6	4.22	8.05
C_2	9.64	2.10	4.61	9.64
$C_3^=$	35.9	33.8	60.9	35.9
C_3	14.3	4.20	5.11	14.3
C_4	4.91	1.63	1.14	4.91
i-C_4	1.49	5.35	0.22	1.49
$C_4^=$	17.8	18.2	13.9	17.8
C_5^+	0.45	0.79	0.78	0.45
Aromatics	5.50	19.1	8.57	5.50
Ar. distribution (%)				
Benzene	29.9	62.3	32.2	29.9
Toluene	41.1	14.6	33.8	41.1
Xylene	2.80	2.60	3.06	2.80
Ethylbenzene	25.1	10.3	17.6	25.1
C_9^+ aromatics	1.67	10.1	13.4	1.67

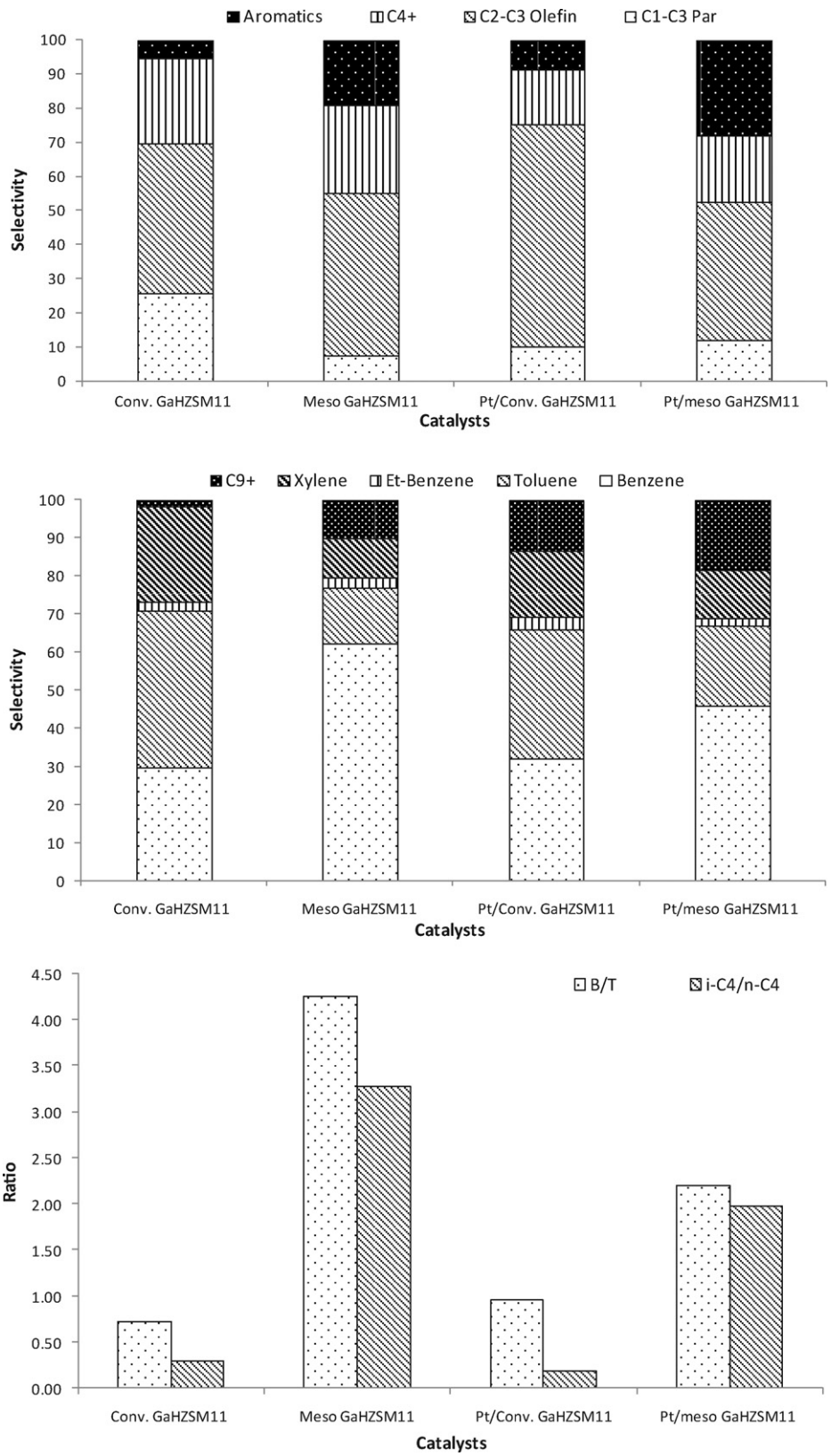

Fig. 7. Products distribution, aromatic distribution and ratio of benzene/toluene and *i*-C_4/*n*-C4 over conventional and mesoporous Ga-containing HZSM-11 catalysts at same conversion level of C_6.

In order to explain the differences observed in the product patterns over the above mentioned catalysts a probable reaction mechanism has been proposed in Fig. 8. The aromatization of n-hexane can occur through two different routes (Fig. 8) i.e. cracking/dehydrogenation or dehydrocylization. Generally in the presence of acidic zeolites, cracking reaction is the main reaction [58] resulting in the production of short-chain paraffins and olefins. The olefins can undergo oligomerization to produce oligomers,

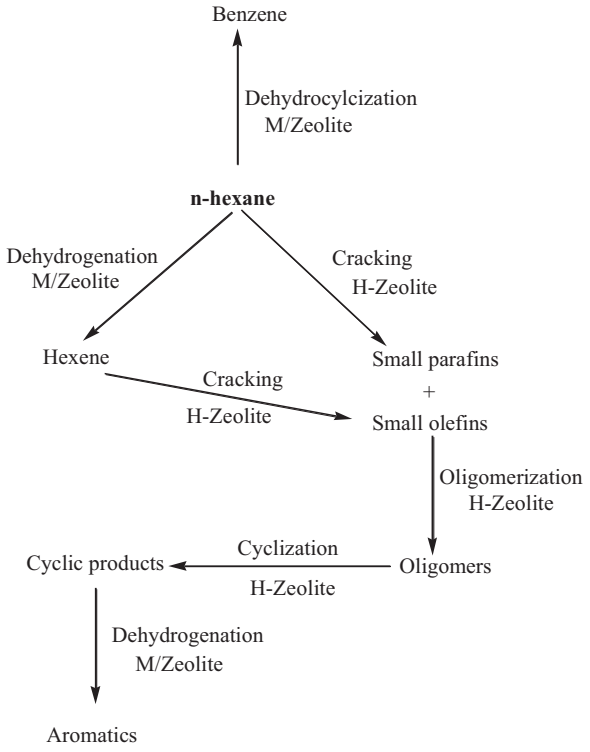

Fig. 8. A probable reaction mechanism during hexane aromatization (M: metal).

which can further undergo cyclization and dehydrogenation to produce aromatics. Whenever some metals are present in the catalysts then dehydrogenation reaction also occur to produce hexene, which is highly reactive and undergo cracking reaction producing smaller olefins and subsequent reactions. In this way, metal impregnated zeolites act as bi-functional catalyst and increase the aromatic yield. Whenever aromatics are produced from cracking/dehydrogenation route (Fig. 8) then toluene is always produced in large amount as compared with benzene. However, there is a chance that metal incorporated zeolites can also cause the dehydrocyclization of *n*-hexane [59] resulting in production of benzene directly.

High ratio of benzene/toluene has indicated that dehydrocyclization process is more favorable on mesoporous GaZSM-11 as compared with conventional GaZSM-11. This can be connected with expected shortening of the contact time due to the presence of mesopores. The dehydrocyclization process results in the formation of large amount of benzene as reported for Pt/KL zeolite [60]. Tauster et al. [61] and Derouane et al. [62] have ascribed the unique feature of Pt/KL to the geometric characteristics of the catalysts. The structure of catalyst orients the hexane molecule in the channels in such a way that it favors the C_1–C_6 closure for dehydrocyclization process. The mesopores present in mesoporous GaZSM-11 also favor isomerization of *n*-butane resulting in production of more isobutane.

3.3.2. Promoter role of platinum

It has been observed that addition of platinum (0.5 wt%) resulted into higher conversions as well as higher selectivity to aromatic products over all catalysts investigated. Platinum has very high dehydrogenation/hydrogenation activity. Therefore, an addition of platinum enhances the dehydrogenation reactions and results in a higher activity as well as higher aromatic selectivity. It was reported [63] that incorporation of platinum into gallium zeolites or gallosilicates favors the formation of the bimetallic particles during reduction. The gallium atoms incorporated in the zeolite favor the stabilization of bimetallic particles inside the zeolite framework and result into higher dehydrogenation and aromatization activity.

Table 6
Aromatization of *n*-hexane over Ga-containing HZSM-5 at 540 °C, atmospheric pressure, LHSV of 3.6 h^{-1}, and TOS of 5 h.

Catalysts	AlZSM-5 (86)	Galloaluminosilicate Ga,AlZSM-5(84)	Pt/galloaluminosilicate, Pt/Ga,AlZSM-5(84)
Conversion (%)	44.7	49.4	55.3
Aromatic (Ar) yield (%)	3.74	5.04	6.12
Product selectivity (%)			
C_1	2.24	2.16	1.39
$C_2^=$	10.9	10.6	7.10
C_2	10.2	9.88	14.3
$C_3^=$	22.0	24.3	29.7
C_3	24.5	20.4	17.1
C_4	6.02	5.59	3.85
i-C_4	2.67	2.83	1.32
$C_4^=$	12.4	13.4	13.7
C_5^+	0.89	0.83	0.44
Aromatics	8.21	10.1	11.1
Ar. distribution (%)			
Benzene	15.3	14.1	12.3
Toluene	46.4	42.5	43.6
Xylene	2.80	3.03	2.47
Ethylbenzene	27.7	33.8	33.5
C_9^+ aromatics	7.79	6.51	8.21

3.3.3. Effect of zeolite structure

The ZSM-5 and galloaluminosilicate (Ga,AlZSM-5) together with corresponding Pt catalysts were tested for *n*-hexane aromatization and results have been compared with that of conventional GaZSM-11 catalysts. The results are presented in Table 6. It was observed that the conversion of n-hexane over galloaluminosilicate Ga,AlZSM-5 was the highest (49%) while that of GaZSM-11 was the lowest (25%) (Table 4). The aromatic yield was also observed to be the highest over galloaluminosilicate Ga,AlZSM-5 while it was comparable over AlZSM-5 and conventional GaZSM-11. The platinum incorporation resulted in an increase in the C_6 conversion for all three zeolites. The order of conversion of *n*-hexane over all catalysts, with or without platinum was same as galloaluminosilicate (Ga,AlZSM-5) > ZSM-5 > conventional GaZSM-11. The product distribution at the same conversion level of hexane is presented in Table 7 and Fig. 9. It was observed that the selectivity to aromatic

Table 7
n-Hexane aromatization over Pt promoted Ga-containing HZSM-5 at the same conversion level (540 °C, atmospheric pressure, and TOS of 5 h).

Catalysts	AlZSM-5 (86)	Galloaluminosilicate Ga,AlZSM-5(84)	Pt/galloaluminosilicate, Pt/Ga,AlZSM-5(84)
Conversion (%)	21.2	20.9	22.0
Aromatic (Ar) yield (%)	0.07	0.26	0.56
Product selectivity (%)			
C_1	2.09	1.97	1.69
$C_2^=$	7.99	8.14	8.08
C_2	11.5	10.3	10.5
$C_3^=$	32.6	35.3	36.9
C_3	19.1	17.8	16.6
C_4	6.03	5.36	4.57
i-C_4	0.96	1.46	1.03
$C_4^=$	18.9	17.9	17.7
C_5^+	0.45	0.48	0.42
Aromatics	0.34	1.22	2.52
Ar. distribution (%)			
Benzene	22.9	25.5	14.4
Toluene	77.1	53.4	49.5
Xylene	0.00	0.00	3.58
Ethylbenzene	0.00	21.8	32.6
C_9^+ aromatics	0.00	0.00	0.00

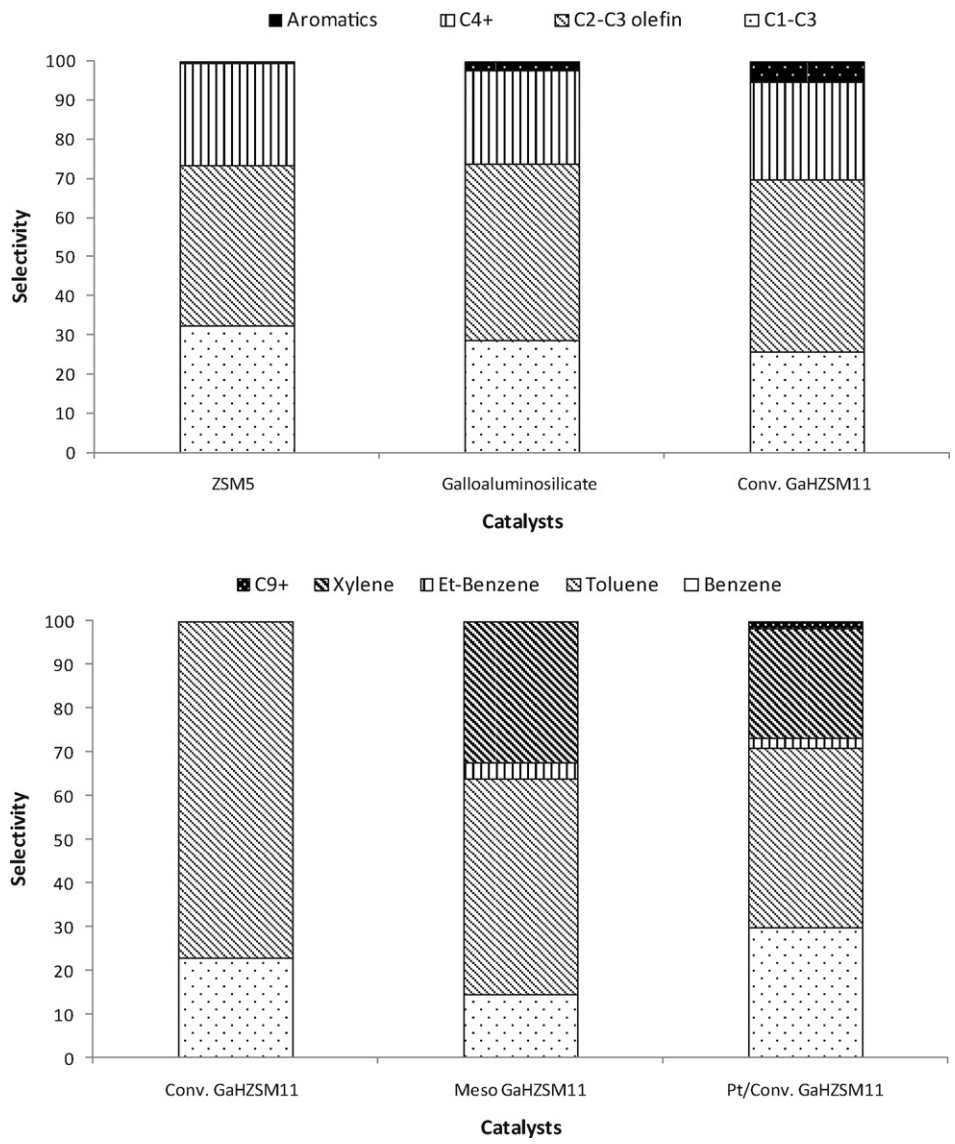

Fig. 9. Products distribution and aromatic distribution over Ga-containing HZSM-5 at same conversion level of C_6.

Table 8
Propane aromatization over Ga-containing zeolites 540 °C, atmospheric pressure, G.H.S.V. of 1600 h^{-1}, and TOS of 5 h.

Catalysts	AlZSM-5 (86)	Galloaluminosilicate Ga,AlZSM-5(84)	Conventional GaHZSM-11(94)	Mesoporous GaHZSM-11(61)
Conversion (%)	5.00	5.10	1.30	10.3
Aromatic (Ar) yield (%)	0.70	1.30	0.10	6.40
Product selectivity (%)				
C_1	29.9	28.9	9.10	9.42
$C_2^=$	27.2	21.6	7.82	6.82
C_2	10.2	8.21	0.69	6.76
$C_3^=$	4.34	4.41	20.5	3.65
C_4	5.85	5.02	13.8	3.40
$C_4^=$	6.01	5.38	12.4	3.62
C_5^+	2.08	1.68	25.7	3.66
Aromatics	14.4	24.7	9.98	62.7
Ar. distribution (%)				
Benzene	18.3	26.5	10.8	28.3
Toluene	36.8	40.5	11.9	24.6
Xylene	2.04	3.27	4.51	1.72
Ethylbenzene	20.8	21.0	24.1	13.4
C_9^+ aromatics	22.1	8.65	48.7	32.0

products was the highest over conventional GaZSM-11. Similar results have been reported by Zhang et al. [64]. They have reported a higher selectivity of ZSM-11 than ZSM-5 during aromatization of *n*-hexene. Most probably, pore structure of the zeolites plays an important role in the increase in the selectivity to aromatic products. The ZSM-5 and ZSM-11 zeolites exhibit only little geometric differences existing in their intersections [65]. Both MFI and MEL type zeolites have three dimensional channels with dimensions about 0.55 nm. The MFI topology consists of intersecting straight and sinusoidal channels, whereas the MEL topology has only intersectional straight channel. Consequently the transport of molecules is much faster in the case of ZSM-11 resulting in higher selectivity.

3.3.4. C_3 aromatization

Propane aromatization was carried out over conventional and mesoporous GaZSM-11, and compared with galloaluminosilicate Ga,AlZSM-5. The results are presented in Table 8. It was observed that all zeolites studied exhibited very low conversion in propane aromatization. It was observed that the conversion of ZSM-5 and galloaluminosilicate Ga,AlZSM-5 were comparable. However, selectivity of aromatics over galloaluminosilicate Ga,AlZSM-5 was much higher (25%) than that of parent ZSM-5 (14%). It indicates the importance of extra-framework Ga species in the reaction mechanism leading to aromatic products. The conversion of propane over GaZSM-11 increased from 1% to 10% after desilication. The aromatic yield also increased from 0.1 to 6.4%. A similar trend was observed during hexane aromatization due to the combined effect of the intracrystalline mesoporosity and the presence of extra framework Ga species in mesoporous GaZSM-11. The higher catalytic conversion of all catalysts during hexane aromatization can be explained based on thermodynamics. It is well established that the aromatization of alkane is thermodynamically more favorable with for paraffins with increasing chain length [66].

4. Conclusion

Desilication of GaZSM-11 using alkaline solutions leads to the development of intracrystalline mesoporosity within the structure, as evident by XRD and N_2 sorption measurements. There were only slight change in the number and properties of acid sites upon desilication. The *n*-hexane and propane aromatization conversion over Ga-containing ZSM-11 increased upon desilication. The conversion was further increased upon the addition of Pt. The aromatization of *n*-hexane increased in the following order, Pt/mesoporous GaZSM-11 ≫ Pt/conventional GaZSM-11 ≫ mesoporous GaZSM-11 > conventional GaZSM-11. The better activity can be attributed to the improved accessibility to the active extra framework Ga species owing to the generation of mesoporosity inside zeolite particles and shortening of the contact time. The mesoporous GaZSM-11 resulted into higher benzene/toluene and *i*-butane/*n*-butane ratios as compared with the conventional GaZSM-11.

Acknowledgments

The authors would like to express their appreciations to King Abdulaziz City for Science and Technology for their financial support under project No. 12-3MT. The financial support made by King Abdullah University of Science and Technology (KAUST) (Award No. K-C1-019-12) is highly appreciated. The authors would like also to extend their appreciation to the support from King Fahd University of Petroleum and Minerals.

References

[1] K. Otto, 22nd World LP Gas Forum, October 8th, Rio de Janeiro, Brazil, 2009.
[2] H.G. Franck, J.W. Stadelhofer, Industrial Aromatic Chemistry , Springer, Berlin, Heidelberg, New York, 1988.
[3] Y.V. Joshi, K.T. Thomson, J. Catal. 246 (2007) 249–265.
[4] M. Guisnet, N.S. Gnep, F. Alario, Appl. Catal. 89 (1992) 1–30.
[5] R. Fricke, H. Kosslick, G. Lischke, M. Richter, Chem. Rev. 100 (2000) 2303–2405.
[6] G. Caeiro, R.H. Carvalho, X. Wang, M.A.N.D.A. Lemos, F. Lemos, M. Guisnet, F. Ramoa Ribeiro, J. Mol. Catal. A 255 (2006) 131–158.
[7] H. Kitagawa, Y. Sendoda, Y. Ono, J. Catal. 101 (1986) 12–18.
[8] J. Kanani, N. Kawata, Appl. Catal. 55 (1989) 115–122.
[9] G.L. Price, V. Kanazirev, J. Catal. 126 (1990) 267–278.
[10] (a) P. Meriaudeau, C. Naccache, J. Mol. Catal. 59 (1990) L31–L36;
(b) P. Meriaudeau, S.B. Abdul Hamid, C. Naccache, J. Catal. 139 (1993) 679.
[11] E. Iglesia, J.E. Baumgartner, G.L. Price, J. Catal. 134 (1992) 549–571.
[12] (a) C.R. Bayense, A.J.H.P. van der Pol, J.H.C. van Hoff, Appl. Catal. 72 (1991) 81–98;
(b) C.R. Bayense, J.H.C. van Hoff, Appl. Catal. 79 (1991) 127–140.
[13] Y. Ono, K. Kanae, J. Chem. Soc. Faraday Trans. 87 (1991) 669–675.
[14] (a) N.S. Gnep, J.Y. Doyemet, M. Guisnet, J. Mol. Catal. 45 (1988) 281–284;
(b) M. Guisnet, N.S. Gnep, Catal. Today 31 (1996) 275–292.
[15] K.M. Dooley, C. Chang, G.L. Price, Appl. Catal. A 84 (1992) 17–30.
[16] (a) B.S. Kwak, W.M.H. Sachtler, J. Catal. 141 (1993) 729–732;
(b) B.S. Kwak, W.M.H. Sachtler, J. Catal. 145 (1994) 456–463.
[17] G.D. Meitzner, E. Iglesia, J.E. Baumgartner, E.S. Huang, J. Catal. 140 (1993) 209–225.
[18] T. Inui, F. Okazumi, J. Catal. 90 (1984) 366–367.
[19] (a) R. Le Van Mao, L. Dufresne, Appl. Catal. 52 (1989) 1–18;
(b) R. Le Van Mao, L. Dufresne, J. Yao, Appl. Catal. 65 (1990) 143–157.
[20] M. Giannetto, A. Montes, N.S. Gnep, A. Florentino, P. Cartraud, M. Guisnet, J. Catal. 145 (1994) 86–95.
[21] S. Jia, S. Wu, Z. Meng, Appl. Catal. A 103 (1994) 259–268.
[22] V.R. Choudhary, A.K. Kinage, C. Sivadinarayana, P. Devadas, S.D. Sansare, M. Guisnet, J. Catal. 158 (1996) 34–50.
[23] N. Kumar, L.-E. Lindfors, Appl. Catal. A 147 (1996) 175–187.
[24] K.J. Chao, S.P. Sheu, L.-H. Lin, J. Genet, M.H. Feng, Zeolites 18 (1997) 18–24.
[25] C.F. Cheng, H. He, W.Z. Zhou, J. Kinowski, J.A.S. Goncalves, L.F. Gladden, J. Phys. Chem. 100 (1996) 390–396.
[26] K.T. Leth, A.K. Rovik, M.S. Holm, M. Broson, H.J. Jakobsen, J. Skibsted, C.V. Christensen, Appl. Catal. A 348 (2008) 257–265.
[27] C.W.R. Engelen, J.P. Wolthuizen, J.H.C. van Hooff, Appl. Catal. 19 (1985) 153–163.
[28] N.S. Gnep, J.Y. Doyemet, A.M. Seco, F. Ramao Ribeiro, M. Guisnet, Appl. Catal. 35 (1987) 93–108.
[29] T. Mole, J.R. Anderson, G. Geer, Appl. Catal. 17 (1985) 141–154.
[30] H. Brendt, G. Lietz, J. Volter, Appl. Catal. 146 (1996) 351–363.
[31] K. Aristirova, Kh. Dimitrov, K. Dyrec, K.H. Hallmeier, Z. Popova, S. Witkowski, Appl. Catal. A 81 (1992) 15–26.
[32] T. Komatsu, M. Mesuda, T. Yashima, Appl. Catal. A 194–195 (2000) 333–339.
[33] W. Li, S.Y. Yu, G.D. Meitzner, E. Iglesia, J. Phys. Chem. C 105 (2001) 1176–1184.
[34] J. Guo, H. Lou, H. Zhao, L. Zheng, X. Zheng, J. Mol. Catal. A 239 (2005) 222–227.
[35] E.S. Shpiro, D.P. Shevchenko, O.P. Tkachenko, R.V. Dmitriv, Appl. Catal. 107 (1994) 147–164.
[36] I. Nowak, J. Quartararo, E.G. Derouane, J.C. Vedrine, Appl. Catal. A 251 (2003) 107–120.
[37] N. Al-Yassir, M.N. Akhtar, S. Al-Khattaf, unpublished data.
[38] J.C. Groen, J.A. Moulijn, J. Perez-Ramirez, J. Mater. Chem. 16 (2006) 2121–2131.
[39] M. Hartmann, Angew. Chem. Int. Ed. 43 (2004) 5880–5882.
[40] S. Donk, A.H. Janssen, J.H. Bitter, K.P. de Jong, Catal. Rev. 45 (2003) 297–319.
[41] M. Ogura, S.H. Shinimiya, J. Tateno, Y. Nara, E. Kikuchi, M. Matsukata, Chem. Lett. (2000) 882–883.
[42] J. Čejka, S. Mintova, Catal. Rev. 49 (2007) 457–509.
[43] Z. Pavlačková, G. Košová, N. Žilková, A. Zukal, J. Čejka, Stud. Surf. Sci. Catal. 162 (2006) 905–912.
[44] J.-B. Koo, N. Jiang, S. Saravanamurugan, M. Bejblová, Z. Musilová, J. Čejka, S.-E. Park, J. Catal. 276 (2010) 327–334.
[45] P. Wu, D. Nuntasri, J. Ruan, Y. Liu, M. He, W. Fan, O. Terasaki, T. Tatsumi, J. Phys. Chem. B 108 (2004) 19126–19131.
[46] A. Corma, M.J. Diaz-Cabanas, J. Martinez-Triguero, F. Rey, J. Rius, Nature 418 (2002) 514–517.
[47] Y. Song, X. Zhu, Y. Song, Q. Wang, L. Xu, Appl. Catal. A 302 (2006) 69–77.
[48] (a) B. Gil, S.I. Zones, S.J. Hwang, M. Bejblová, J. Čejka, J. Phys. Chem. C 112 (2008) 2997–3007;
(b) N. Žilková, M. Bejblová, B. Gil, S.I. Zones, A.W. Burton, C.Y. Chen, Z. Musilova, J. Čejka, J. Catal. 266 (2009) 79–91.
[49] Database of Zeolite Structures, April 10. http://www.iza-structure.org/database/, 2011.
[50] B. Zheng, W. Hua, Y. Yue, Z. Gao, J. Catal. 232 (2005) 143–151.
[51] X. Zhu, L.L. Lobban, R.G. Mallinson, D.E. Resasco, J. Catal. 271 (2010) 88–98.
[52] D. Ohayon, R.L. Van Mao, D. Ciaravino, H. Hazel, A. Cochennec, N. Rolland, Appl. Catal. A. 217 (2001) 241–251.
[53] J.C. Groen, L.A.A. Peffer, J.A. Moulijn, J. Perez-Ramirez, Colloid Surf. A 241 (2004) 53–58.
[54] V.R. Choudhary, K. Mantri, C. Sivadinarayana, Microporous Mesoporous Mater. 37 (2000) 1–8.

[55] I. Kanai, N. Kawata, Appl. Catal. 55 (1989) 115–122.
[56] A.Y. Khodakov, L.M. Kustov, T.N. Bondarenko, A. Degachev, V.B. Kazansky, K.M. Minachev, G. Borbely, H.K. Beyer, Zeolites 10 (1990) 603–607.
[57] K. Nishi, S. Komai, K. Inagaki, A. Satsuma, T. Hattori, Appl. Catal. A 223 (2002) 187–193.
[58] N. Viswanadham, A.R. Pradhan, N. Ray, S.C. Vishoni, U. Shanker, T.S.R.P. Rao, Appl. Catal. A 137 (1996) 225–233.
[59] G. Giannetto, J.A. Perez, R. Sciamanna, L. Garcia, R. Gallasso, R. Monque, Div. Petrol. Chem., Am. Chem. Soc. 36 (1991) 659–667.
[60] K.G. Azzam, G. Jacobs, W.D. Shafer, B.H. Davis, J. Catal. 270 (2010) 242–248.
[61] S.J. Tauster, J.J. Steger, J. Catal. 125 (1990) 387–389.
[62] E.G. Derouane, D.J. Vanderveken, Appl. Catal. A 45 (1988) 15–22.
[63] M.N. Mikhailov, I.V. Mishin, L.M. Kustov, A.L. Lapidus, Microporous Mesoporous Mater. 104 (2007) 145–150.
[64] L. Zhang, H. Liu, X. Li, S. Xie, Y. Wang, W. Xin, Fuel Process. Technol. 91 (2010) 449–455.
[65] P.A. Jacobs, J.A. Martens, J. Weitkamp, H.K. Beyer, Faraday Discuss. Chem. Soc. (1981) 353–369.
[66] N. Viswanadham, G. Muralidhar, T.S.R.P. Rao, J. Mol. Catal. A 223 (2004) 269–274.